

Spatial Distribution of Material Properties in Load Bearing Femur as Characterized by Evolutionary Structural Optimization

Hadi Latifi¹, Lev Lafayette¹ and Mehmet Bilgen^{2,*}

¹Centre for Innovative Structures and Materials, School of Civil, Environmental and Chemical Engineering, RMIT University, GPO Box 2476, Melbourne, VIC3001, Australia

²Biophysics Department, Faculty of Medicine, Adnan Menderes University, 09100 Aydin, Turkey

Abstract: This work aims to simulate bone formation under natural loading using evolutionary structural optimization. Unlike material elimination by hard-kill approach applied previously, the current presentation implements material replacement defined as soft-kill method. A numerical analysis platform was developed and finite element model of sheep femur was constructed using computer tomography data. Quadruple material properties governing soft medullary canal, cancellous as well as plexiform and haversian cortical structures were considered as the main material constituents of the femur. An iterative algorithm was designed for determining the spatial distribution of these tissue types throughout the femur. The model initially started with a homogenous plexiform design and iteratively converged to a final state with heterogeneous density profile, nearly similar to a natural femur. The inefficient regions were gradually changed with mechanically lower grade and lighter tissues and thus the final construct had the least weight but still supported the load. The convergence was achieved successfully. The tissue types were distributed in a mechanically optimum fashion to counteract the applied forces. The resulting internal material assignments provided insights into the structural remodeling of femur within the context of Wolff's law. Using the developments, bone formation can be simulated numerically under different mechanical loading conditions. Such investigations may provide useful information about the vulnerability of bone as its material properties change with osteoporosis or the fracture risk as a result of malfunction in muscles attached to the femur.

Keywords: Bone formation, evolutionary structural optimization, soft-kill, Wolff's law, finite element analysis.

1. INTRODUCTION

Understanding bone formation and remodeling with age, mechanical loading and other factors has been the focus of research efforts in the past [1-4]. Computer simulations, especially finite element (FE) modeling, have played important role in uncovering adaptation mechanisms and relationships between the property, structure and function of bone [5-8]. FE analysis of bone formation has been further advanced with the introduction of structural optimization concept from engineering [9-11]. This numerical platform was applied to sheep femur subjected to mechanical loading imposed by normal gait [12-14]. Initial femur design was constructed by assigning a constant material composition as described by the stiffest elasticity throughout the femur. Structural evolution from the initial design to the final formation was achieved iteratively using hard-kill method where mechanically inefficient elements in supporting the structure were eliminated from the model iteratively [11]. Eventually, the model converged to a form capturing the basic topology of the real femur, i.e. nearly a hollow shaft. The final design contained minimal amount of bone material while meeting the load requirements.

The assumption that material property would remain constant throughout the femur during the remodeling process was a limitation of the hard-kill approach.

In reality, bone is structurally a complex matrix consisting of mainly 4 different materials: mechanically superior, stiff and dense plexiform tissue of cortical bone; mechanically inferior, less stiff haversian tissue of cortical bone, porous tissues of cancellous bone, and soft tissue of medullary canal. As opposed to the hard-kill, we hypothesized that adapting soft-kill concept into the structural evolution process would lead to a final formation of bone with minimal mass, but still satisfying the original design constraints. This study was therefore initiated to develop and implement the necessary components of a numerical analysis platform required for remodeling bone formation using structural evolution based on the soft-kill, and demonstrate the merits of the approach. Specifically, the platform combined material replacement/change optimization routine with FE analysis to evaluate the macroscopic behavior of sheep femur subjected to dominant muscle forces common to gait. During the optimization process under the soft material replacement (MR), the density property assigned to the FE model was updated iteratively to produce structurally evolving femur to a final design. In the following, we give the details of the numerical simulations and discuss the outcomes in the context of

*Address correspondence to this author at the Biophysics Department, Faculty of Medicine, Adnan Menderes University, 09100 Aydin, Turkey, Tel: +90 537 284 0149; Fax: +90 256 212 0146; E-mail: mehmet.bilgen@yahoo.com

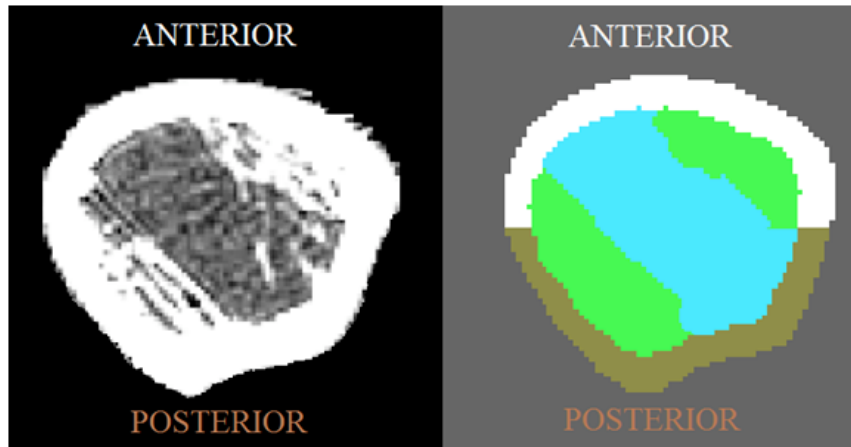


Figure 1a: Axial CT image of femur bone of sheep at the mid shaft level. **b:** Masked image of femur bone color coded to show its cortical haversian (brown), and cortical plexiform (white), cancellous (green) and medullary canal (light blue) sections.

evolutionary bone remodeling and functionality using MR approach.

2. MATERIALS AND METHODS

The specific bone that was employed in this study has been described earlier [11]. Here, we give specific details relevant to the MR operations. The real femur used for the FE modeling was from the left side of a two year old sheep. It was imaged using a Computer Tomography (CT) scanner (Siemens SOMATOM Sensation 4) in axial (transverse) view along the femur shaft using the following parameters: 140kVP, $0.4 \times 0.4 \text{ mm}^2$ in-plane pixel resolution and 0.6mm slice thickness.

2.1. Estimation of the Material Properties of Femur Bone

The CT images were imported in mhd format to a Matlab (Mathworks, Inc, USA) code written in house and processed for determining the material density properties of the femur bone. Materials constituting the composition of bone were grouped and their densities were represented relatively [15, 16]. Specifically, the tissue in the medullary canal was associated with void, cancellous tissue was considered as forming the porous bone, and haversian and plexiform bone were considered as being parts of the cortical tissue. Following this grouping, axial CT image of the femur, as in Figure 1, was processed for segmenting out its cortical, cancellous and medullary sections by applying standard image intensity thresholding [11]. The cortical ring was further divided into half at the mid coronal plane to distinguish between the inferior haversian tissue developed posterior and the harder plexiform

tissue located anterior to the femur. Average Hounsfield unit values were then calculated from the selected regions of interest as 238, 1893, 2768 and 3786, respectively. These readings were then further mapped proportionally into the values 10^{-5} , 0.538, 0.731 and 1 g/mm^3 for representing the relative material density properties of the corresponding tissues normalized between 0 to 1 [17]. Similarly, the stiffness values were mapped as 35×10^{-15} , 5.45, 13.672 and 35 GPa, respectively [18].

2.2. Numerical Analysis

The implementation of the MR based optimization process for bone remodeling was algorithmically described by the flowchart in Figure 2. The steps of the algorithm is similar to the one presented earlier in [11], but when looked closely the decision mechanism governing the material swapping instead of element elimination can be seen as the major difference between the two. The procedures for the MR optimization process mainly involved four modules:

- 1- Constructing an initial FE model of the femur,
- 2- Assigning mechanical loads at the model boundaries,
- 3- Conducting the FE analysis, calculating strain energy density (SED) for each element of the FE model and producing SED map and,
- 4- Making a decision for reassigning the material properties to the elements based on their SED ranks.

Modules 3 and 4 repeated as part of the optimization process. The post processing code for

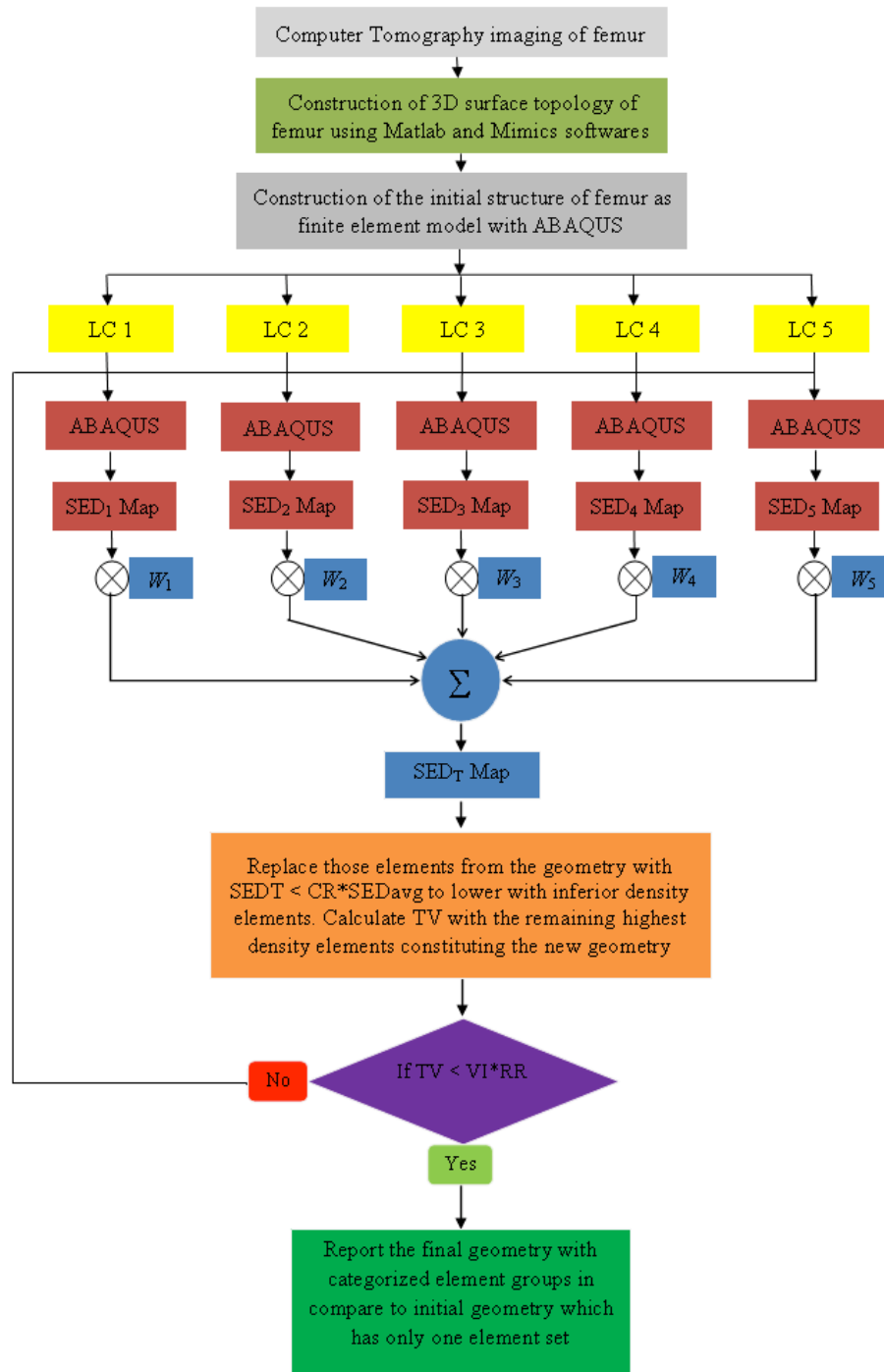


Figure 2: Flowchart of the iterative structural MR optimization performed during the study. The FE computational parts of the analysis were carried out with ABAQUS and indicated by boxes in red color. The blue colored boxes indicate the post processing carried out using Fortran code. The acronyms are as follows; LC: load cases described as boundary condition on the model, ABAQUS: finite element modelling Solver and SED calculator, SED_i ($i=1,..5$): strain energy density of special load case of FE, SED_T : summation of SED_i being multiplied by relevant weight factor of W_i ; SED_{avg} : average strain energy density over all elements structure, CR: convergence ratio and set to be 0.001, TV: total volume, VI: initial volume of design with highest density and RR: rejection ratio set to be 0.5 as volume constraint and first convergence criteria. (W_1, W_2, W_3, W_4, W_5) are weight factors associated with the five loading conditions on the femur and were set to (0.35, 0.19, 0.25, 0.15, 0.06).

deciding the density change was written in Visual Fortran (VFortran 90 + Visual studio 2005, Microsoft Corporation, New York, USA).

2.3. Constructing the FE Model

The sheep femur was numerically constructed by following the procedures described previously [11, 20].

First, the 3D surface topology of the femur was extracted from the CT images. From this data, a mesh was produced using Mimics software (Materialise, Leuven, Belgium). From the mesh, a FE model was created using ABAQUS 6.10-2 software (Dassault Systemes, Villacoublay, France). In this model, the whole bone was filled completely with tetrahedron shaped elements with an average edge length of 1mm. When the aspect ratio of an element was of poor quality (<0.1), this element was combined with its neighbor manually to improve mesh quality.

Initially, the whole bone was considered to be uniformly made up of hard plexiform tissue and thus all

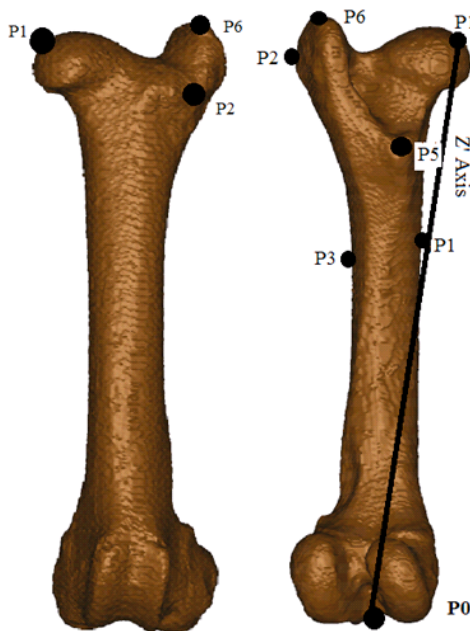


Figure 3: Schematic of the initial FE model of the sheep femur (left side) from anterior and posterior views. The marked black points indicate mechanical loading (or boundary condition) applied on the bone. Black line is the indicator of musculoskeletal coordinate axis (Z). Note that this initial design was completely filled with plexiform tissue.

of the model elements were assigned accordingly with relative material density 1g/mm^3 and the corresponding elastic modulus of 35 GPa. This construct constituted the initial homogeneous design, as showed in Figure 3.

2.4. Mechanical Loading

The model in Figure 3 was mechanically loaded on its boundaries with major musculoskeletal forces identified from earlier gait analysis of clinically healthy sheep [12-14]. These dominant forces were applied in target locations; with magnitude and direction as seen in Figure 4 and the contribution of each was appropriately weighted with a factor W (0.35, 0.19, 0.25, 0.15 or 0.06) respectively, in the algorithm (Figure 2) [14]. The distal end of the femur was fixed and supported on its condyle.

2.5. Material Optimization

The mechanical response of the numerically simulated femur was investigated using the iterative MR optimization algorithm in Figure 2. The process started with the initial FE design and applied load configuration. Optimization was defined as

$$\text{Minimize: } C = \mathbf{u}^T \mathbf{K} \mathbf{u} \quad (1)$$

Under the constraint of: $V^* - \sum V_i x_i = 0$

x_i = density of all inferior material groups (three groups with densities less than 1) arranged according to SED ranking (10^{-5} , 0.5 or 0.731) for $1 \leq i \leq N$.

In Eq. (1), N denotes the total number of elements of the FE model. \mathbf{K} is the stiffness matrix of the whole structure and \mathbf{u} is the global displacement vector. $\mathbf{u}^T \mathbf{K} \mathbf{u}$ denotes the stored energy to be optimized under the given volume constraint. The objective is to efficiently distribute the bone density and materials properties throughout the structure according to the necessities.

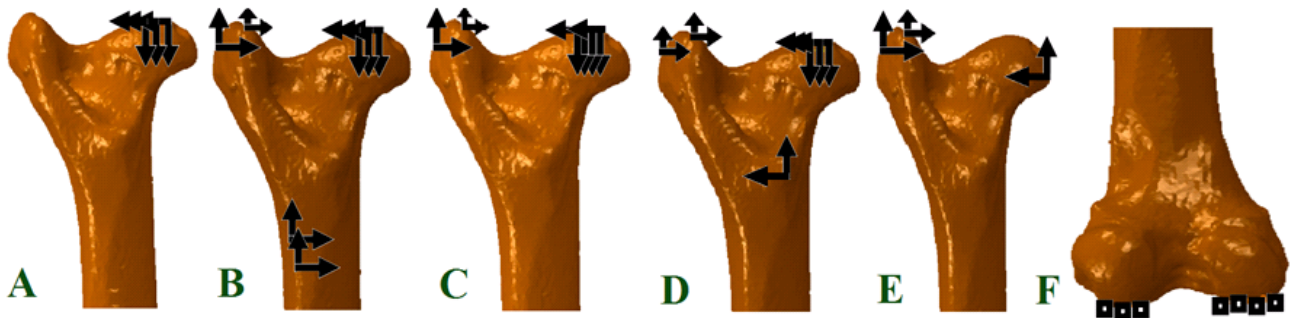


Figure 4: Five different load cases applied to the simulated bone under normal gait. **A:** Fully compressed at femur head, **B:** Heel strike, **C:** Stance, **D:** Mid-toe off and **E:** Fall while the condyle was encastered, as shown in **F**.

V_i is the volume of each individual element (3D meshed tetrahedron) and V^* is the total volume to be populated with the three inferior density groups; plexiform, haversian, cancellous and medullary canal tissues. V^* starts with 10% of the initial total volume of the bone and increases to maximum 90% during the intermediate intervals with 5% increment at each step. The normalized artificial density variable x_i denotes the density of the i^{th} element which is determined according to the SED range ranking. In each step of the optimization, a density of x_i was assigned each element and its relative elastic modulus was calculated according to the following relation;

$$E(x_i) = E_{plexi} x_i^p \quad (2)$$

where E_{plexi} is Young's modulus of the plexiform bone (35 GPa) and p is a penalty exponent predefined as 3 according to the literature [21].

2.6. Sensitivity and Element Optimization Ranking

Sensitivity of the objective optimization function in relation to the change in the i^{th} element properties was identified by the partial differentiation $\partial C / \partial x_i$, which would result in the SED [21]. The SED at the integration point was chosen as volumetric optimization criterion [22]. To avoid discontinuities and checking board pattern, Normalized Nodal SED with $r = 3$ filter radius selected to determine which density group each node belongs to.

2.7. Element Ranking and Convergence Criteria

In each step of the optimization process, the computations were performed with the predefined loadings. According to the SED results, the design elements were ranked into four density groups and relative material properties were reassigned. The convergence test started from the second iteration since the design history was needed to check the design stability. At each iteration, two convergence constraints were tested: (a) volume constraint V^* , and (b) stability of the design.

In each iteration (after the 2th one), prior to the design stability check, the volume constraint V^* was checked first. Then, if less than 1% of the elements optimized in this iteration (properties were changed between four defined groups) in comparison to the previous one, design was considered as being stabilized and converged. To be realistic and for preventing computational errors, surface boundary

elements were allowed to change only between the two densest groups of haversian or plexiform tissue.

3. RESULTS

The characteristic features of the FE model constructed as the initial design were summarized in Table 1. The model had fine mesh consisting of elements with an average of 1mm edge length. The volume of the meshed femur was 153,104mm³ which was comparable to the volume 152,326mm³ estimated from the CT data. Running the algorithm in Figure 2 took about 46 hours and the optimization process converged to a stable solution after 118 iterations. The convergence rates and behavior of the material switching in iterations had similar pattern to those reported in the previous engineering topology optimization studies [23, 24].

Table 1: Characteristics of the FE Model of the Femur

Mean edge length	1mm
Volume	153,104mm ³
Node number	185,376
Element number	1,876,153

Figure 5 shows the femur designs obtained at iterations 60 and 118. As the iteration progressed, the elements internal to the bone were replaced by mechanically inferior tissue while those elements closer to the femur surface remained as plexiform tissue. This feature has been displayed better in transverse views in Figure 6. The material properties were distributed non-uniformly across the simulated femur. Those

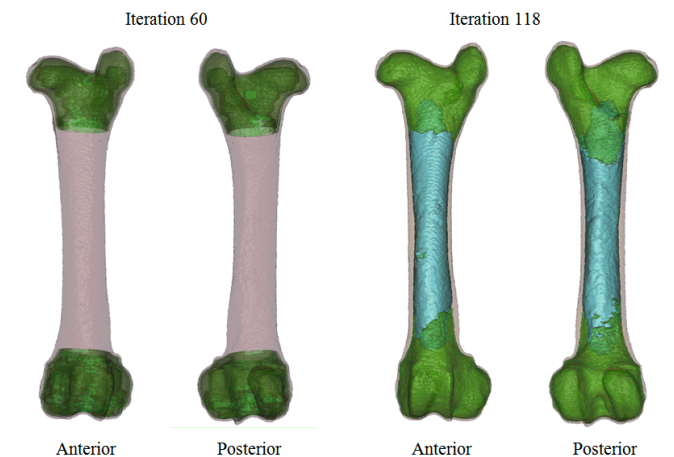


Figure 5: Femur designs at iterations 60 and 118 of the MR optimization procedure. Green: porous bone, brown: cortical bone (both haversian and plexiform groups) and light blue: medullary canal.

sections which have been changed to inferior elements inherently represent mechanically weak regions.

The CT images in Figure 6 shows the cross sections of the real femur at the locations where the

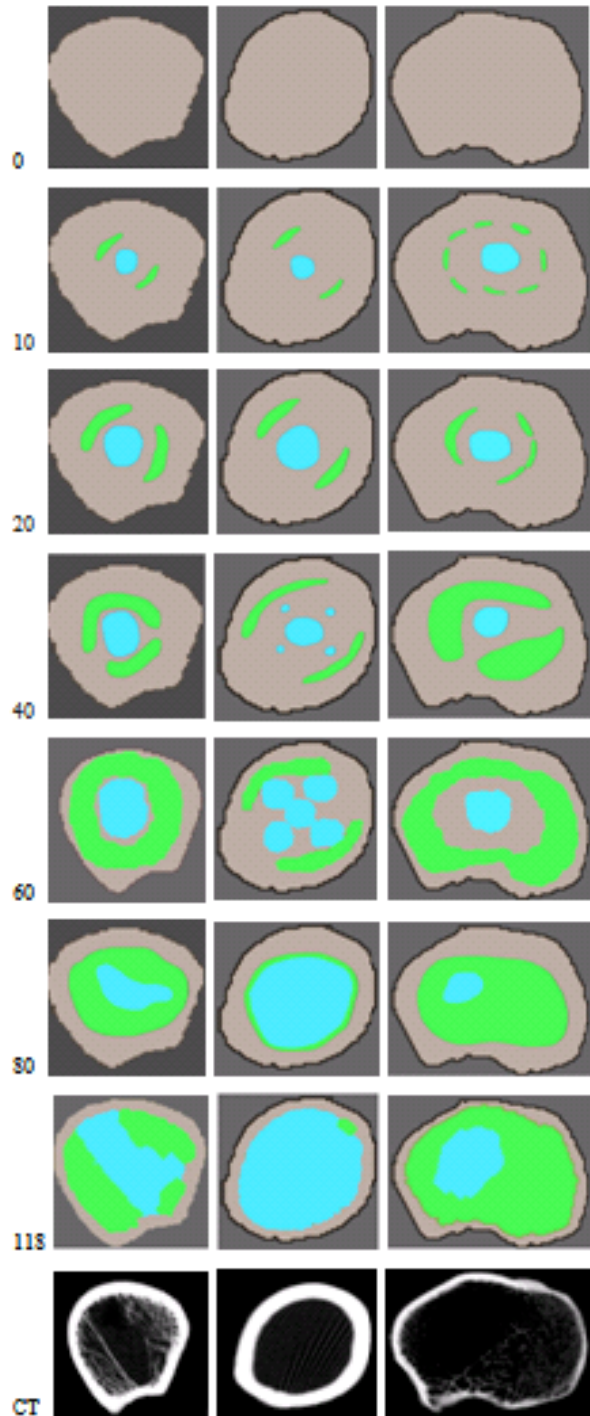


Figure 6: Cross sectional visualization of the femur at the top, middle and down sections when viewed from the proximal to distal direction at iterations 0, 10, 20, 40, 60 and 118 of the MR optimization procedure. Corresponding axial CT images were provided at the bottom as reference for verifying the predictions of the MR optimization.

simulations were produced. Based on qualitative visual evaluation, the close similarity of the model predictions to the profiles of the real bone confirms the accuracy and reliability of the analysis of the bone formation and remodeling with the MR based evolutionary structural optimization method.

4. DISCUSSION

Wolff's theory indicates that bone under healthy condition adapts to loads under which it has been conditioned. Although paradox exists, the theory still inspires biomechanical research in orthopedics [25, 26]. Bone becomes tougher/thicker or lighter depending on the internal stress induced within. Simple changes on loading lead to modifications in bone density and structural orientation [27]. One way to evaluate such a response is to use numerical tools developed for structural optimization. Using such a tool, porous pattern in human femur was shown to simulate a microscopically optimized structure [28]. In this study, we took a macroscopic view and employed MR approach to investigate the formation of tissue types and densities in remodeling of sheep femur under mechanical loading exerted by muscles attached to it during normal walk. It has been suggested that, for reducing the optimization time and calculation cost, the material inhomogeneity can be factored in, but orthotropic properties can be omitted in the global FE analysis of femur [29]. This simplification was also taken into account in the current study. The efforts collectively led to the implementation of the iterative algorithm in Figure 2 and the construction of the numerical femur model in Figure 3. Starting with a completely uniform initial design and mechanical loading in Figure 4, the model was iteratively modified step by step. During the process, spatially inefficient elements were revealed and their properties were changed with inferior but lighter material to eventually result in a design with the least weight in Figure 6. These results were in line with the mechanical principles of Wolff and confirmed by the design principle of the process of MR implemented in this study.

CT-based FE modeling was typically used to assess the macroscopic behavior of bone under loading and reported to be acceptably accurate [30, 31]. This study used automatic mesh generation directly from CT images. The bone formation was predicted through local strain energy density. Because of muscle attachments to the surface, FE results showed the outer boundary of the femur as populated with

plexiform and haversian tissues. The porous bone represented by light green and marrow represented by light blue in Figures 5 and 6 seemed to act as an impact energy absorber for the femur. Porous bone concentrated mostly at the proximal and distal metaphyses of the femur.

According to the MR analysis presented above, bone seems to be a mechanically optimized graded structure. This research can be extended to a comparative study of failure and risk analysis for bone under muscle malfunction or other physical bone irregularities to predict the probable failure sections due to the resulting changes in bone density.

The present analysis considered the femur being loaded statically by only major muscle groups, as such was the case in the literature [32, 33]. The distal end of the femur was fixed, rather than loaded by the muscles or tendons attached to this end. This was a limitation of this study as it lacked dynamic or cyclic loading as well as inclusion of other muscles. A fully dynamic FE model under more flexible muscle forces may bring better understanding and details of bone remodeling in time sequence [20].

In FE modeling, the spatial dependence of the elasticity variation initially was not taken into consideration and the whole femur was assigned a constant elastic modulus corresponding to plexiform bone to simulate the most inefficient /heaviest design case scenario. However, heterogeneous, instead of homogenous elastic modulus assigned to the porous and medullary canal could have made the model better mimic the real initial conditions of the femur.

CONCLUSION

CT data alone provide information about the femur's topology and biomechanical properties of its material constituents. This information makes it feasible to construct an initial FE model of femur and subsequently to perform iterative material replacement optimization. Simulations under different load conditions allow determining whether the material distribution has been assigned in a mechanically optimized fashion and thus provide insights into the structural remodeling of femur within the context of Wolff's law of bone transformation where the tissue types are distributed in a mechanically optimum fashion to counteract the applied forces. Also such investigations may reveal the vulnerability of bone due to changes in its material properties associated with

osteoporosis or fracture risks as a result of malfunction in muscles attached to it.

REFERENCES

- [1] Robling AG, Castillo AB and Turner CH. Biomechanical and molecular regulation of bone remodeling. Annual Review of Biomedical Engineering 2006; 8: 455-498.
<http://dx.doi.org/10.1146/annurev.bioeng.8.061505.095721>
- [2] Boccaccio A, Ballini A, Pappalettere C, Tullo D, Cantore S and Desiate A. Finite element method (FEM), mechanobiology and biomimetic scaffolds in bone tissue engineering. Int J Biol Sci 2011; 7: 112-132.
<http://dx.doi.org/10.7150/ijbs.7.112>
- [3] Boyle C and Kim IY. Three-dimensional micro-level computational study of Wolff's law via trabecular bone remodeling in the human proximal femur using design space topology optimization. J Biomech 2011; 44: 935-942.
<http://dx.doi.org/10.1016/j.jbiomech.2010.11.029>
- [4] Evans AL, Paggiosi MA, Eastell R and Walsh JS. Bone Density, Microstructure and Strength in Obese and Normal Weight Men and Women in Younger and Older Adulthood. J Bone Miner Res 2015; 30(5): 920-928.
<http://dx.doi.org/10.1002/jbmr.2407>
- [5] Fischer KJ, Johnson JE, Waller AJ, McIlff TE, Toby EB and Bilgen M: MRI-based modeling for radiocarpal joint mechanics: validation criteria and results for four specimen-specific models. J Biomech Eng 2011; 133: 101004.
<http://dx.doi.org/10.1115/1.4005171>
- [6] Piccinini M, Cugnoni J, Botsis J, Zacchetti G, Ammann P and Wiskott A: Factors affecting subject-specific finite element models of implant-fitted rat bone specimens: critical analysis of a technical protocol. Comput Methods Biomech Biomed Engin 2013; 17: 1403-1417.
<http://dx.doi.org/10.1080/10255842.2012.736502>
- [7] Machado MM, Fernandes PR, Cardadeiro G and Baptista F: Femoral neck bone adaptation to weight-bearing physical activity by computational analysis. Journal of Biomechanics 2013; 46: 2179-2185.
<http://dx.doi.org/10.1016/j.jbiomech.2013.06.031>
- [8] Morgan TG, Bostrom MP and van der Meulen MC: Tissue-level remodeling simulations of cancellous bone capture effects of in vivo loading in a rabbit model. J Biomech 2014. <http://www.ncbi.nlm.nih.gov/pubmed/25579991>
- [9] Li Q, Steven GP and Xie YM. Evolutionary structural optimization for stress minimization problems by discrete thickness design. Computers and Structures 2000; 78: 769-780.
[http://dx.doi.org/10.1016/S0045-7949\(00\)00057-2](http://dx.doi.org/10.1016/S0045-7949(00)00057-2)
- [10] Steven G, Querin O and Xie M. Evolutionary structural optimisation (ESO) for combined topology and size optimisation of discrete structures. Computer Methods in Applied Mechanics and Engineering 2000; 188: 743-754.
[http://dx.doi.org/10.1016/S0045-7825\(99\)00359-X](http://dx.doi.org/10.1016/S0045-7825(99)00359-X)
- [11] Latifi H, Xie YM, Huang X and Bilgen M. Computational simulations of bone remodeling under natural mechanical loading or muscle malfunction using evolutionary structural optimization method. Engineering 2014; 6: 113-126.
<http://dx.doi.org/10.4236/eng.2014.63015>
- [12] Hutzschenreuter PO, Sekler E and Faust G. Loads on muscles, tendons and bones in the hind extremities of sheep—a theoretical study. Anatomia Histologia Embryologia-Journal of Veterinary Medicine Series C-Zentralblatt Fur Veterinarmedizin Reihe C 1993; 22: 67-82.
<http://dx.doi.org/10.1111/j.1439-0264.1993.tb00343.x>
- [13] Bergmann G, Graichen F and Rohlmann A. Hip joint forces in sheep. Journal of Biomechanics 1999; 32: 769-777.
[http://dx.doi.org/10.1016/S0021-9290\(99\)00068-8](http://dx.doi.org/10.1016/S0021-9290(99)00068-8)

- [14] Agostinho F, Rahal S, Araujo FA, Conceicao R, Hussni C, El-Warrak A, et al. Gait analysis in clinically healthy sheep from three different age groups using a pressure-sensitive walkway. *BMC Veterinary Research* 2012; 8: 87-94. <http://dx.doi.org/10.1186/1746-6148-8-87>
- [15] Hangartner TN and Overton TR. Quantitative measurement of bone density using gamma-ray computed tomography. *Journal of Computer Assisted Tomography* 1982; 6: 1156-1162. <http://dx.doi.org/10.1097/00004728-198212000-00017>
- [16] Cong A, Buijs JO and Dragomir-Daescu D. In situ parameter identification of optimal density-elastic modulus relationships in subject-specific finite element models of the proximal femur. *Med Eng Phys* 2011; 33: 164-173. <http://dx.doi.org/10.1016/j.medengphy.2010.09.018>
- [17] Hamed E, Lee Y and Jasiuk I. Multiscale modeling of elastic properties of cortical bone. *Acta Mechanica* 2010; 213: 131-154. <http://dx.doi.org/10.1007/s00707-010-0326-5>
- [18] Zannoni C, Mantovani R and Viceconti M. Material properties assignment to finite element models of bone structures: a new method. *Medical Engineering and Physics* 1999; 20: 735-740. [http://dx.doi.org/10.1016/S1350-4533\(98\)00081-2](http://dx.doi.org/10.1016/S1350-4533(98)00081-2)
- [19] Lengsfeld M, Schmitt J, Alter P, Kaminsky J and Leppke R. Comparison of geometry-based and CT voxel-based finite element modelling and experimental validation. *Medical Engineering and Physics* 1998; 20: 515-522. [http://dx.doi.org/10.1016/S1350-4533\(98\)00054-X](http://dx.doi.org/10.1016/S1350-4533(98)00054-X)
- [20] Latifi MH, Gantheil K, Rukmanikanthan S, Mansor A, Kamarul T and Bilgen M. Prospects of implant with locking plate in fixation of subtrochanteric fracture: experimental demonstration of its potential benefits on synthetic femur model with supportive hierarchical nonlinear hyperelastic finite element analysis. *BioMedical Engineering OnLine* 2012; 11: 1-18. <http://dx.doi.org/10.1186/1475-925X-11-23>
- [21] Huang X and Xie YM. Bi-directional evolutionary topology optimization of continuum structures with one or multiple materials. *Computational Mechanics* 2009; 43: 393-401. <http://dx.doi.org/10.1007/s00466-008-0312-0>
- [22] Zuo ZH and Xie YM. Evolutionary topology optimization of continuum structures with a global displacement control. *Computer-Aided Design* 2014; 56: 58-67. <http://dx.doi.org/10.1016/j.cad.2014.06.007>
- [23] Huang X and Xie YM. Convergent and mesh-independent solutions for the bi-directional evolutionary structural optimization method. *Finite Elements in Analysis and Design* 2007; 43: 1039-1049. <http://dx.doi.org/10.1016/j.finel.2007.06.006>
- [24] Huang X and Xie YM. Optimal design of periodic structures using evolutionary topology optimization. *Structural and Multidisciplinary Optimization* 2008; 36: 597-606. <http://dx.doi.org/10.1007/s00158-007-0196-1>
- [25] Johnson KA. Wolff's law continues to inspire orthopaedic research. *Vet Comp Orthop Traumatol* 2014; 27: V-VI. <http://dx.doi.org/10.3415/vcot-13-12-0142>
- [26] Hammer A. The paradox of Wolff's theories. *Ir J Med Sci* 2015; 184: 13-22. <http://dx.doi.org/10.1007/s11845-014-1070-y>
- [27] Tsubota K, Suzuki Y, Yamada T, Hojo M, Makinouchi A and Adachi T. Computer simulation of trabecular remodeling in human proximal femur using large-scale voxel FE models: Approach to understanding Wolff's law. *J Biomech* 2009; 42: 1088-1094. <http://dx.doi.org/10.1016/j.jbiomech.2009.02.030>
- [28] Jang IG and Kim IY. Computational study of Wolff's law with trabecular architecture in the human proximal femur using topology optimization. *J Biomech* 2008; 41: 2353-2361. <http://dx.doi.org/10.1016/j.jbiomech.2008.05.037>
- [29] Baca V, Horak Z, Mikulenka P and Dzupa V. Comparison of an inhomogeneous orthotropic and isotropic material models used for FE analyses. *Med Eng Phys* 2008; 30: 924-930. <http://dx.doi.org/10.1016/j.medengphy.2007.12.009>
- [30] Cristofolini L, Schileo E, Juszczak M, Taddei F, Martelli S and Viceconti M. Mechanical testing of bones: the positive synergy of finite-element models and in vitro experiments. *Philosophical Transactions of the Royal Society a-Mathematical Physical and Engineering Sciences* 2010; 368: 2725-2763. <http://dx.doi.org/10.1098/rsta.2010.0046>
- [31] Kim HS, Park JY, Kim NE, Shin YS, Park JM and Chun YS. Finite element modeling technique for predicting mechanical behaviors on mandible bone during mastication. *Journal of Advanced Prosthodontics* 2012; 4: 218-226. <http://dx.doi.org/10.4047/jap.2012.4.4.218>
- [32] Yosibash Z, Padan R, Joskowicz L and Milgrom C. A CT-based high-order finite element analysis of the human proximal femur compared to in-vitro experiments. *Journal of Biomechanical Engineering-Transactions of the ASME* 2007; 129: 297-309. <http://dx.doi.org/10.1115/1.2720906>
- [33] Horch RA, Gochberg DF, Nyman JS and Does MD. Non-invasive predictors of human cortical bone mechanical properties: T-2-Discriminated H-1 NMR compared with high resolution X-ray. *PLoS ONE* 2011; 6: e16359. <http://dx.doi.org/10.1371/journal.pone.0016359>

Received on 28-03-2016

Accepted on 02-06-2016

Published on 13-07-2016

DOI: <http://dx.doi.org/10.15377/2409-9848.2016.03.01.3>

© 2016 Latifi et al.; Avanti Publishers.

This is an open access article licensed under the terms of the Creative Commons Attribution Non-Commercial License (<http://creativecommons.org/licenses/by-nc/3.0/>) which permits unrestricted, non-commercial use, distribution and reproduction in any medium, provided the work is properly cited.